5328 *Macromolecules* **2009**, *42*, 5328–5338
DOI: 10.1021/ma802503s

Macromolecules
ARTICLE

Dynamic Light Scattering Study of Concentrated Triblock Copolymer Micellar Solutions under Pressure

A. F. Kostko,*,†,‡ J. L. Harden,§ and M. A. McHugh†

†*Department of Chemical and Life Science Engineering, Virginia Commonwealth University, Richmond, Virginia 23284,* ‡*Department of Physics, St. Petersburg State University of Refrigeration and Food Engineering, St. Petersburg, 191002, Russia, and* §*Department of Physics, University of Ottawa, Ottawa, ON K1N 6N5 Canada*

Received November 7, 2008; Revised Manuscript Received June 7, 2009

ABSTRACT: The results from a dynamic light scattering study of concentrated aqueous systems of polyethylene oxide−polypropylene oxide−polyethylene oxide triblock copolymer (PEO−PPO−PEO, Pluronic F108) are reported at pressures to 2500 bar and temperatures from 0 to 110 °C. The pressure−temperature ($P-T$) phase behavior for this micellar system exhibits several phase transformations at high concentrations including a transition from a liquid to a gel phase and a subsequent re-entrant transition from the gel phase to a liquid phase with increasing temperature. The gel phase region is bounded at low temperatures by a liquid-to-gel phase transition curve that increases in pressure with increasing temperature, eventually exhibits a maximum in pressure, and then at high temperatures rapidly decreases as the temperature is further increased. The high temperature branch of this curve represents a gel-melting transition. Aqueous F108 samples are doped with latex probe nanoparticles to facilitate the characterization of the local viscosity and also to serve as a reference for the measurement of the light intensity scattered by the Pluronic systems. Both the intrinsic collective dynamics of the Pluronic systems and the diffusive dynamics of the nanoparticle probes are characterized. The diffusive dynamics of the nanoparticle probes reveal the nonmonotonic character of viscosity that results from phase transformations dependent on pressure and temperature. The micellar system scattering intensity, obtained from DLS data through comparison with the light intensity scattered by the probe nanoparticles, increases with heating indicating critical pretransitional behavior of concentration fluctuations on approach to the cloud-point boundary over a broad temperature interval that spans the gel phase temperature range.

Introduction

Polymers consisting of ethylene oxide and propylene oxide monomers display complex behavior in aqueous systems. The nominally hydrophobic interactions of the CH_2 segments of the polymer backbone are compensated by polar interactions between oxygen atoms and water molecules. The solvation of water by these polymers is thought to be a consequence of the formation of a delicate network of structured water molecules associated with the oxygen atoms in these polymers.[1,2] With increasing temperature, this water network is progressively disrupted, inhibiting the solvation of the polymer in water. Thus, aqueous solutions of these polymers exhibit a lower critical solution temperature. Since polypropylene oxide (PPO) has one more CH_2 unit per monomer repeat unit than polyethylene oxide (PEO), the range of solubility of PPO is significantly reduced compared to PEO and therefore PPO phase separates from water at a lower temperature. As a consequence, with increasing temperature, water rapidly becomes a selective solvent for copolymers of PEO and PPO.[3] The focus in the present paper is on the system behavior of triblock PEO−PPO−PEO copolymers, commonly known as Pluronics (BASF trade name). These nontoxic triblock copolymers are important for a variety of applications including drug and gene delivery.[3−5] The central PPO block is water-soluble at low temperatures but becomes more hydrophobic and less water-soluble as the temperature is increased. The PEO end blocks, however, are significantly more soluble in water and only slowly become less water-soluble upon heating. As with other block copolymer systems, a relative change in solvent quality eventually leads to microphase separation of Pluronic aqueous systems and the formation of mesophases with symmetry dictated by the molecular architecture (e.g., cubic, cylindrical, lamellar, and bicontinuous phases.[6−9])

The present paper reports the results of a dynamic light scattering investigation of the aqueous PEO−PPO−PEO copolymer (Pluronic F108, 80% EO and 20% PO, with a reported molecular weight of 14.6 kg/mol) system that undergoes microphase separation into suspensions of spherical micelles with dense PPO cores and relatively thick, brush-like PEO coronae. At sufficiently high polymer concentrations these micellar systems exhibit several structural transitions, including a transition to a gel-like cubic crystalline phase,[6−10] characteristic of a concentrated suspension of repulsive soft colloidal particles existing in a finite temperature range that is sensitive to copolymer concentration and system conditions (e.g., the concentration and type of added salts.[11,12])

A few authors have reported that pressure affects micellar behavior in Pluronic aqueous systems.[13−15] Interestingly, an increase in the pressure suppresses the aggregation of unimers in a manner reminiscent of the dissolution of micellar aggregates that occurs in response to a decrease in temperature. This suppression of micellization by pressure presumably has its origins in the enhanced solubility of the more hydrophobic PPO block in water at elevated pressure. Mortensen et al. observed[13] that increasing pressure actually causes the micellar crystalline phase to melt, which is an inverted pressure dependence, analogous to the

*Corresponding author. E-mail: afkostko@yahoo.com.

 Published on Web 07/02/2009

inverted temperature dependence of micellar crystals that melt with cooling. Mortensen et al.[13] argue that the increase in entropy upon heating, as demanded by the tenets of thermodynamics, occurs in spite of the increased system order at the length scale of micelles (~10 nm). One possibility is that disruption of the water structure around these ethoxylated polymers at elevated temperatures accounts for the required entropy increase. In this picture, elevated pressure would tend to stabilize the water structure around the polymers, thereby inhibiting the formation of micelles and their ordered phases. Another possible mechanism of entropy production discussed in this paper is the enhancement of molecular-scale thermal fluctuations in response to increasing temperature.

Studies of the dynamics in these systems could shed light on this issue. Various experimental methods, including neutron spin echo,[16] light scattering,[17−27] mechanical rheometry,[18,19,28−31] and fluorescence lifetime techniques[32−34] have been used at ambient pressure to study aspects of the system dynamics in aqueous Pluronic systems. In this paper light scattering studies of the dynamic properties of concentrated Pluronic solutions are reported over broad $P-T$ ranges. Dynamic light scattering (DLS) is used to determine the phase behavior, micellar dynamics, and the local viscosity at pressures to 2500 bar and temperatures from 0 to 110 °C. The DLS data obtained in this study are compared with neutron spin echo data obtained by Yardimci et al.[16] for the same micellar system. Moreover, to probe simultaneously the local viscosity of these Pluronic systems at various pressures and temperatures, a microrheology method is employed based on DLS measurements of light scattered from a dilute suspension of nanoparticle probes doped into the solution. In addition to providing information about the local viscoelastic properties of the solutions, light scattered by the probe particles provides a reference scattering intensity, which facilitates the determination of the intensity of intrinsic scattering by the micellar system with changes in pressure and temperature. Information on the temperature dependence of the intensity of scattering by the micellar system is obtained from the DLS data, where the contributions of the different dynamic modes to the total scattering intensity can be separated.

Experimental Methods

A. Sample Preparation. Pluronic F108 (pastille), obtained from BASF Inc. as a gift, is a triblock PEO−PPO−PEO copolymer with 80 mass % PEO and a molecular weight of ~14.6 kg/mol. Millipore pure water (18 MΩ·cm), filtered with a syringe-mounted 0.02 μ Whatman Anotops filter, is used as the solvent to create a 0.20 g/cm^3 F108 solution that is sufficiently concentrated to form gel phase.[16] At ambient conditions, homogeneous mixing of solid F108 in water is hindered by the formation of a gel-like, supersaturated layer at the surface of the solid F108. Thus, to minimize the solution preparation time the F108-water solution is kept in a refrigerator and subjected to periodic gentle shaking and mixing. Even though the subambient temperature in the refrigerator is far from the gel-transition boundary, the total dissolution of F108 usually takes a day or two depending on the efficiency of mixing. After dissolution the concentration is adjusted to 0.20 g/cm^3 with additional filtered water. Preliminary light scattering experiments are conducted on neat F108 aqueous solutions in a glass cylinder at ambient pressure. A tiny amount of polystyrene latex (87 nm diameter, Duke Scientific Corp.) is then doped into the sample before the sample is charged to the high-pressure light scattering cell.

B. High-Pressure Dynamic Light Scattering. Details are given elsewhere[35,36] on the high-pressure scattering cell and the DLS apparatus. A light beam from a solid state laser (200 mW DPSS Nd:YAG, Coherent Inc., $\lambda = 532$ nm) is incident on the input window of the scattering cell and is focused at the center of the cell. The scattering cell has sapphire windows for the incident and transmitted laser beam, and windows at 36, 45, 90, and 135° for scattered light. Scattered light is split and delivered to two photomultipliers (PMTs) to provide pseudocrosscorrelation that eliminates afterpulses. The light detecting optics with PMTs are mounted on a goniometer arm positioned at the angles corresponding to the optical cell output windows. DLS measurements are performed with an ALV-5000/E FAST correlator, which accumulates the intensity correlation functions, $g_2(t)$. In addition, the time-averaged intensity at each scattering angle is available for static light scattering analysis.

The F108 solution is compressed by an internal piston displaced with Millipore filtered water (18 MΩ·cm) delivered from a second cell also containing an internal piston displaced with tap water in a pressure generator. This tandem scattering-pressurizing cell setup provides an additional barrier to eliminate even small levels of tap water contamination of the F108 solution that could result from microleaking through the piston O-ring. The solution temperature is controlled within ±0.2 K and the system pressure is measured with a transducer/display to within ±5 bar.

The CONTIN regularization procedure of the inverse Laplace transform (ALV software) is used to analyze $g_2(t)$ to obtain the decay time distribution, $H(\tau)$. It was more convenient to obtain $H(\tau)$ rather than fitting the correlation function to several exponentials because the number of modes in the distributions varied depending on temperature and pressure. The magnitude of the distribution $H(\tau)$ for a certain value of the decay time, τ, is proportional to the partial scattering intensity, which is characterized by this particular decay time. Thus, $H(\tau)$ provides information about the relative intensity of the dynamic modes represented in this intensity-weighted distribution. The dynamic modes attributed to the micellar system and to the latex probe particles do not overlap and are easily identified in $H(\tau)$. These modes are characterized by the mean peak positions (average decay-times) and by the intensity contributions of these peaks. The intensity contributions of the micellar modes, H_m, and of the latex particles mode, H_p, are obtained from $H(\tau)$.

To estimate the intensity of scattering by the micellar system we must account for the scattered intensity of the latex probe particles. The intensity of scattering by the latex particles is proportional to their volume concentration, size, and the square of the difference between the refractive indices of the polystyrene latex particles and of the solution, reduced by the particle form factor at finite scattering angles. In this study we neglect the pressure-induced increase of the latex volume fraction driven by the compressibility of the aqueous micellar system. We also neglect possible pressure-induced changes in the size of the polystyrene particles. The refractive index of the latex particles is close to 1.59 and the refractive index of the solution is close to that of water, which is significantly lower. Therefore, small pressure and temperature induced variations of the water refractive index should not have a significant effect on the large refractive indices difference. Likewise, also neglected are any variations of the scattered intensity caused by possible changes of the form factor of latex probe particles. The pressure and temperature dependence of the solution refractive index is estimated using high-pressure density data[37] and the temperature and density dependence of the refractive index of pure water.[38] With these estimates, it can be shown that the variation of the particle scattering intensity barely exceeds 20% in the entire range of experimental conditions, and therefore, this variation is neglected from further consideration in our calculations.

The intrinsic scattering intensity, I_m, of the F108 micellar system can be calculated as $I_m = I_p \times H_m/H_p$, where I_p is the scattering intensity of the latex probe particles. It is possible to extract I_m and I_p from the total scattering intensity using the value of H_m/H_p if all other contributions to total intensity, except I_m and I_p, are negligible. However, since variations of I_p

are neglected in the present experiments, I_m is now $I_m = H_m/H_p$ where the approximately constant factor of I_p is simply omitted, which implies $I_p = 1$. This approach eliminates the statistical error of the total scattering intensity measurement, although it introduces some systematic error related to the neglected variations of I_p. It is important to note also that the ratio H_m/H_p is independent of any variations of the power of the incident laser beam. Thus, the common significant problem of intensity measurement is eliminated using DLS data and the reference scattering intensity of the latex probe particles. Uncertainty of the evaluation of $I_m/I_p = H_m/H_p$ inevitably increases when the contribution of one mode dominates over the other in the total intensity, namely, when $I_m/(I_m + I_p)$ is small or is close to 100%. For the data represented in this paper the ratio $I_m/(I_m + I_p)$ ranges from 2% to 97%.

The diffusive mode of the latex probe particles provides information about the viscosity of the Pluronic phases at nanoscopic length scales. The validity of our microrheology measurements with polystyrene latex probe particles depends on the stability of this aqueous suspension at high pressure and elevated temperature. Alargova et al.[39] observed an aggregation of polystyrene latex spheres in water at pressures below 280 bar when the temperature exceeds 280−300 °C. These temperatures are well above 110 °C, the highest operating temperature used in the present study. However, since the operating pressures in the present study are significantly higher than 280 bar, further DLS measurements were performed by the present authors (to be published elsewhere) with polystyrene latex particles in pure water at pressures to 2600 bar and verified that there was no evident change in particle size within 10% error bars that could be caused by compression, aggregation, or swelling, and that could affect the conclusions reported in the present study. Likewise, the reproducibility of the data reported in the present study at various pressures and temperatures suggests that irreversible aggregation of the latex particles does not occur. A recent combined high-pressure small angle neutron scattering and dynamic light scattering study by Meier, et al.[40] showed that the pressure-induced changes of silica probe particles in toluene are very small and can be neglected in DLS experiments. Polystyrene latex particles are preferred in the present study as they have a lower specific gravity, 1.1 versus 1.8 g/mL, which is closer to that of water, and they have a higher refractive index, 1.59 versus 1.48, than silica. Also, the higher difference between the refractive indices of polystyrene and water exhibits relatively lower changes due to any variation of water refractive index with pressure and temperature. Consequently, the polystyrene latex probe particles in water have a much lower tendency for sedimentation and a higher intensity of scattering, which is less sensitive to pressure and temperature variations and allows for lower concentration of probe particles.

Results and Discussion

Figure 1 shows typical intensity correlation functions, $g_2(t)$, obtained in this study for liquid and gel states, with and without latex probe particles, for aqueous 0.20 g/cm^3 solutions of F108 at ambient pressure. The diameter of the probe particles, 87 nm, is approximately nine times larger than the hydrodynamic radius of F108 micelles, which is approximately 11 nm.[41] The gel phase is associated with the appearance of "frozen scatterers" in the gel network, a signature of nonergodic behavior by the system announced by a characteristic long-tail background contribution in the correlation function.[42−44] Figure 1 shows that the characteristics of the micellar liquid (21 °C) and the gel state (40 °C) correlation functions for solutions without probe particles are only slightly different and, accordingly, the long-time tail of the correlation function for the Pluronic sample, without latex, in the gel state is rather weak. After doping the solution with latex particles a more dramatic change of correlation function is observed when crossing the gel phase boundary, making it much easier to locate this phase boundary. Decay time distributions for concentrated aqueous Pluronic solutions usually exhibit at least two modes,[17−27] with the number of observable modes depending on experimental conditions. The decay rates (reciprocal of the decay times) of these modes are proportional to the square of the scattering wavenumber, $q = 4\pi n\lambda^{-1} \sin(\theta/2)$, where n is the refractive index of the solution and θ is the scattering angle. This usually indicates that the decay rates are characteristic of diffusion modes. Figure 2 shows a typical example of the decay time distributions, $H(\tau)$, obtained in this study at 21 °C and ambient pressure at three scattering angles and plotted with respect to $q^2\tau$. The diffusive character of the modes is confirmed by the coincidence of the modes at all three scattering angles. However, the diffusive character of all satellite dynamic modes is not checked in detail at each experimental condition.

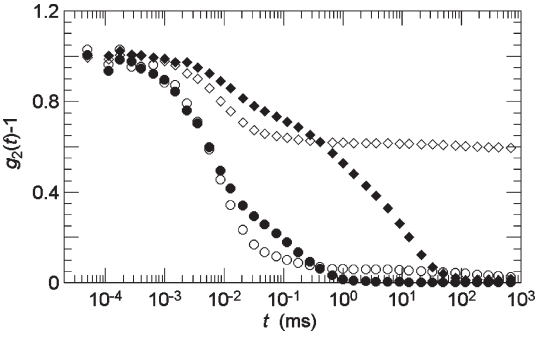

Figure 1. Correlation functions accumulated at ambient pressure for the 0.20 g/cm^3 F108 aqueous system. Only each fifth data point is shown. Solution without latex probe particles: micellar liquid at 21 °C, solid circles; gel at 40 °C, open circles. Solution doped with latex probe particles: micellar liquid at 21 °C, solid diamonds; gel at 40 °C, open diamonds. The long-time tail is truncated for the gel-phase correlation functions. Scattering angle: 90°.

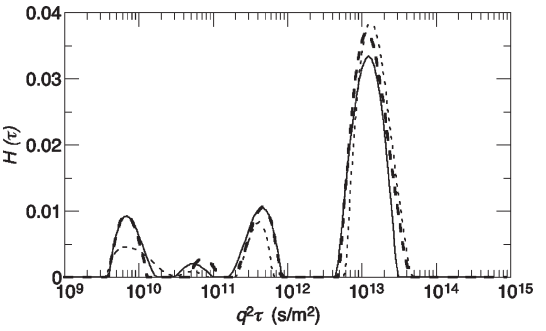

Figure 2. Decay time distributions $H(\tau)$ for the 0.20 g/cm^3 F108 aqueous solution at 21 °C and ambient pressure. Scattering angles: 45°, dots; 90°, solid line; 135°, short dashes.

The slowest mode corresponds to diffusion of latex probe particles, while the other modes originate from light scattered by the F108 solution. The fastest of the latter intrinsic scattering modes (hereafter referred to as the fast mode) is observed in all of our measurements below the cloud-point boundary at 110 °C. The position of the fast mode changes smoothly throughout the entire 0 to 110 °C temperature range and one to 2500 bar pressure range. In contrast, the slower satellite modes shown in Figures 1 and 2 change their location and appearance as the temperature is changed. Their magnitudes are relatively low at high temperatures on approach to the cloud point and at low temperatures corresponding to solutions of individual polymer chains. The focus here is on the dominant intrinsic mode, namely the fast mode, as well as on the diffusive latex probe particle mode. Also discussed is the evolution of the weak satellite dynamic modes with order−disorder phase transitions in the sample.

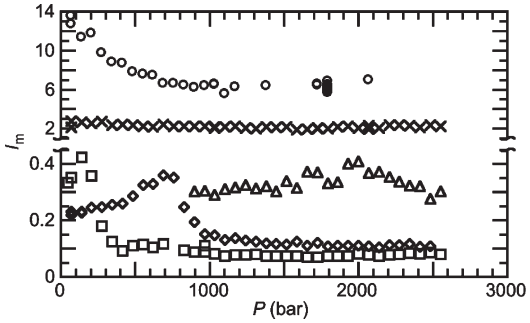

Figure 3. Pressure dependence of the scattering intensity at 90° for the micellar system of 0.20 g/cm^3 F108 aqueous solution: squares, 22 °C; diamonds, 30 °C; triangles, 45 °C; crosses, 92 °C; circles, 102 °C.

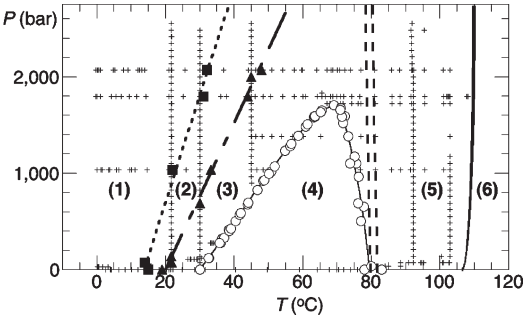

Figure 4. $P-T$ phase diagram for the 0.20 g/cm^3 F108 aqueous solution. (1) Liquid-phase region with individual polymer chains. Critical micellization temperature and pressure − filled squares and dotted line. (2) Liquid-phase region with individual polymer chains and spherical micelles. End of micellization is shown as filled triangles and a long-dashed line. (3) Liquid-phase region with spherical micelles and clusters of micelles. (4) Gel region with cubic crystal-like ordering of spherical micelles. The phase boundary is delimited with a solid line and the data with circles. (5) Liquid, micellar-phase region expected to have rods or worm-like micelles located close to the cloud-point boundary, which is depicted with a solid line. (6) Two-phase region, opaque milk-like suspension of solid polymer in water. The narrow strip shown with the double dashed lines separating regions 4 and 5 is a liquid phase with low viscosity. Crosses indicate pressures and temperatures where DLS data have been obtained.

DLS measurements for both neat and latex-doped solutions were obtained over wide $P-T$ ranges. In the case of latex-doped solution, the measurements were performed in the liquid region of the phase diagram where the behavior of the sample is ergodic. Measurements at the gel-phase boundary, which indicate nonergodic behavior, were made as a means of the phase boundary mapping. Generally, DLS measurements in a nonergodic, gel phase should be performed with ensemble averaging[42] that in practice usually is achieved by sample rotation, which is not possible with our high-pressure DLS cell. Hence, data obtained with latex-doped solutions in the gel phase were used to indicate qualitatively the appearance of the gel phase via the emergence of nonergodic behavior. Note, however, that the contribution by "frozen" scatterers to the scattering intensity for F108 aqueous solutions without latex particles is low, and hence that nonergodic behavior did not significantly affect the interpretation of the data obtained in these time-averaged measurements.

In addition to using the diffusive dynamics as a probe of Pluronic solution behavior, the intensity of scattering by the solutions is also used to characterize their phase behavior. As previously mentioned, the intensity of scattering by the Pluronic chains and their micellar aggregates, I_m, is approximated as $I_m = H_m/H_p$ using the intensity data for the latex probe particles as the reference value. Figure 3 shows intensity data for five temperatures as a function of pressure. At 22, 30, and 45 °C the intensity first increases with pressure exhibiting a maximum, which is followed at 22 and 30 °C by essentially low and almost constant values. Analogous maxima as well as the flat regions are also observed in the temperature dependence of the scattering intensity at low pressure. The flat regions of low and almost constant intensity correspond to solution of individual polymer chains at low temperature and/or elevated pressure. With a decrease of the solvent quality on approach of lower pressures, the intensity I_m starts increasing at the critical micellization temperature/pressure (CMTP) when polymer chains begin to associate into spherical micelles. Following standard procedure,[41,45] the temperature and pressure values corresponding to the salient point at the edge of the flat region are used to map the CMTP on the F108 aqueous solution phase diagram. When the maximal intensity is reached, the process of micellization reaches saturation and terminates. It is assumed that the system becomes a micellar liquid where the majority of polymer chains is assembled in spherical micelles and the micelles are contacting each other. Zhou and Chu[46,47] attribute the scattering intensity maxima observed close to the termination of micellization to the presence of composition heterogeneity of Pluronic chains. This composition heterogeneity results in the formation of a dilute emulsion due to a microphase separation that occurs between the CMT and the termination point of micellization. The temperature and pressure corresponding to the intensity maxima are used to map the line of saturation and termination of micellization on the phase diagram. It is interesting that the maximum in scattered intensity is more pronounced at low temperatures and pressures, which, in agreement with Zhou and Chu, could be attributed to the gradual increase of solubility with pressure of the components that have a tendency to phase separate during the process of micellization. In a recent study,[48] the presence of a diblock fraction in the Pluronic samples is linked also with the crystalline lattice symmetry of the cubic gel.

At 92 and 102 °C, temperatures above those in the gel phase region, the intensity I_m is much higher than at lower temperatures (Figure 3). At 102 °C the intensity at low pressures decreases to a constant value, while at 92 °C the value of I_m is almost independent of pressure. The intensity variation at 102 °C is attributed to the operating in the proximity of the cloud-point temperature, which apparently is lower at low pressure.

The phase diagram is mapped using the $P-T$ dependence of the dynamics of the probe latex particles and of the intrinsic scattered intensity I_m. Figure 4 shows the phase transition boundary of the gel state and the $P-T$ range explored in our experiments. In region 1, a liquid region with individual polymer chains, the scattered intensity does not exhibit detectable temperature dependence. At the critical micellization boundary, $(\partial P/\partial T)_{coexistence} = 120$ bar/K, the scattered intensity begins to increase and eventually reaches a saturation or local maximum value at the terminal micellization line, $(\partial P/\partial T)_{coexistence} = 75$ bar/K. Region 2, between the critical and terminal micellization boundaries, is a liquid-phase region containing individual polymer chains and spherical micelles. Region 3, just beyond the terminal micellization line, is a liquid-phase region containing spherical micelles that occupy the entire volume of the sample. The micelles are suspended in water coexisting with a fraction of individual chains. This liquid phase is a micellar liquid where short-range order is assumed. Our DLS data in region 3 imply that pretransitional clustering of micelles occurs in the nuclei of the gel phase. The pressure trace at 30 °C in Figure 3 illustrates the increase of I_m with decreasing pressure in regions 1 and 2, and the apparent maximum in I_m at the terminal micellization boundary. Region 4 is the crystalline gel phase of ordered spherical micelles, while region 5 is a re-entrant micellar liquid phase. DLS measurements, subsequently discussed in detail, identify the phase boundary between regions 4 and 5 by the rapid increase of the

apparent local viscosity probed by latex particle diffusion and the concomitant emergence of the signature of the nonergodic behavior in the intensity correlation function. The two dashed lines depict a narrow region having a steep drop in viscosity close to the gel melting boundary just over 80 °C. Finally, for sufficiently high temperatures, there is a transition to a phase-separated region 6 consisting of an opaque suspension of solid polymer particles in water.

As shown on the phase diagram, a critical micellization temperature is found at 15 °C at ambient pressure. This critical micellization temperature is in good agreement with the value of 17 °C for an F108 solution, that is calculated from an extrapolation to a concentration 0.20 g/cm^3 from the data reported by Alexandridis et al.[41,49] Our value is also consistent with critical micellization temperature data obtained by calorimetery reported by Lau et al.[50] However, the end-of-micellization data as well as the gelation temperatures reported by Lau et al.[50] for an aqueous 0.20 g/cm^3 solution of F108 at ambient pressure are a few degrees higher than the values reported here, which could be ascribed to some batch-to-batch variation of the F108 samples.

Several features of the $P-T$ phase diagram in Figure 4 are consistent with results reported by Mortensen et al.[13] for aqueous Pluronic F88 solutions. For example, the onset of the temperature of gelation upon heating increases with pressure. The data in the present study are obtained over a larger temperature range than that investigated by Mortensen et al.;[13] they include measurements of the pressure dependence of the high-temperature boundary of the gel region, which is a direct melting transition, and they show the pressure limit for the formation of gel phase. The high-temperature boundary of the gel region exhibits a negative $P-T$ slope, $(\partial P/\partial T)_{\text{coexistence}} \approx -10^3$ bar/K, that is steeper than the slope of the low-temperature gel boundary, $(\partial P/\partial T)_{\text{coexistence}} = 49$ bar/K. Both slopes are determined from tangent lines at ambient pressure. Our observation of the difference between the low- and high-temperature gel phase boundaries is supported implicitly by the results of Li et al.[51] More details are presented on several interesting aspects of the collective dynamics of F108 solutions in various regions of the $P-T$ phase diagram.

Dynamics of Probe Particles. The decay time $\tau_p = 1/(Dq^2)$ of the dynamic mode of latex probe particles is determined by the diffusion coefficient D of the probe particles, which in turn depends on the apparent viscosity, η_{app}, of the solution in the local environment surrounding the particles

$$D = \frac{k_B T}{6\pi\eta_{app} R} \quad (1)$$

where k_B is Boltzmann's constant and R is the hydrodynamic radius of latex probe particles. The apparent viscosity, η_{app}, which is the microviscosity revealed by the motion of probe particles, is obtained from the experimentally determined value of D using eq 1.

Figure 5 shows the effect of pressure on the apparent viscosity, η_{app}. At 22, 30, 45, and 102 °C the value of η_{app} exhibits nonmonotonic behavior with pressure. For 22, 30, and 45 °C, the initial decrease of η_{app} with an increase of pressure is attributed to pretransitional behavior near the gelation boundary. The probe particles slow down as they are trapped in growing gel clusters on approach to the low-temperature boundary of the gel phase with a decrease of pressure. Note that at 22, 30, and 45 °C the evidence of pretransitional behavior is detectable far from the gelation boundary. At 102 °C the initial decrease of η_{app} at low pressures reflects the response of the system on close approach to the cloud-point boundary.

Figure 6 shows the temperature dependence of the viscosity at various pressures. At low temperatures η_{app} decreases

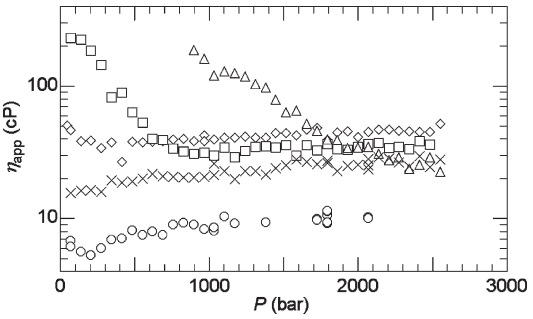

Figure 5. Viscosity, η_{app}, as the function of pressure for the 0.20 g/cm^3 F108 aqueous system: diamonds, 22 °C; squares, 30 °C; triangles, 45 °C; crosses, 92 °C; circles, 102 °C.

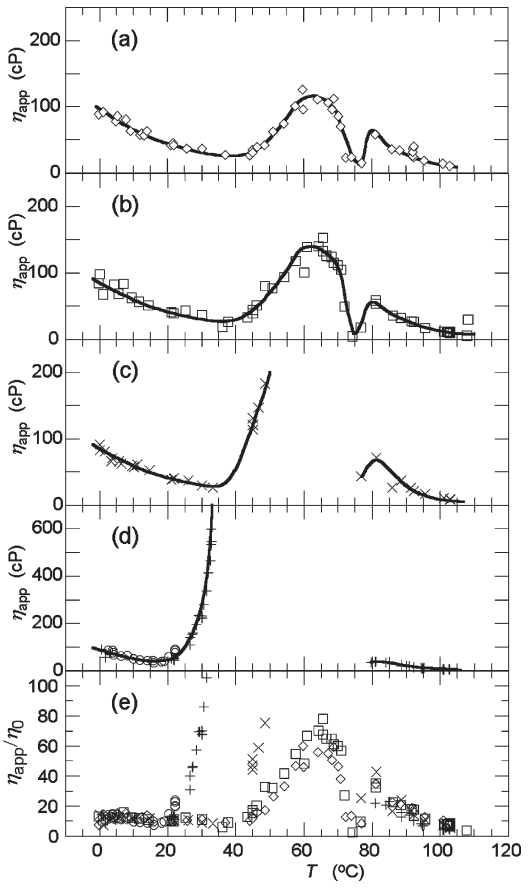

Figure 6. Temperature dependences of the apparent viscosity, η_{app}, for the 0.20 g/cm^3 F108 aqueous system. The lines in these graphs are drawn to aid the eye: (a) diamonds, 2070 bar; (b) squares, 1790 bar; (c) crosses, 1035 bar; (d) circles, ambient pressure; pluses, 70 bar; (e) viscosity, η_{app}, relatively to water viscosity, η_0.

as the temperature increases, presumably due to a typical Arrhenius temperature dependence resembling the dependence of pure water. The Arrhenius behavior of the viscosity is revealed in the lower section of Figure 6 for the viscosity data recast in terms of the ratio of η_{app} to the water viscosity η_0. At low temperatures this ratio is almost constant. In addition to Arrhenius behavior, the viscosity decrease with heating at low temperatures could also be a consequence of the progressive depletion of Pluronic chains in solution as a result of the formation of micelles and a consequence of PPO block shrinkage. This initial decrease is followed by a sharp increase in the viscosity with increasing temperature near the

terminal micellization line depicted in the phase diagram in Figure 4. The temperature-induced increase of viscosity shown in Figure 6 indicates that the probe particles are trapped in growing clusters of micelles on approach to the gel phase boundary. This behavior is similar to the previously discussed pressure-induced viscosity behavior shown in Figure 5. Pretransitional gelation phenomenon begins far from the gel boundary and almost immediately after the terminal micellization line. Thus, the clustering of micelles is observed in almost the entire region 3 of the phase diagram (Figure 4). As intermicellar interactions in this system are repulsive in nature at these temperatures and pressures, this clustering phenomenon is presumably associated with an order−disorder transition driven by the progressive homogenization of the micelle population. As the system is heated at constant pressure, the finite-size clusters of ordered micelles are growing and associating, finally occupying the entire volume of the sample to form a gel phase. Gelation occurs for our sample at pressures below approximately 1720 bar. At pressures over this limit only finite-size micellar clusters are detected in the phase of disordered liquid micellar solution. Accordingly, the viscosity data at 1790 and 2070 bar in Figure 6 exhibit maxima indicating the appearance of a very viscous liquid. These maxima are followed by sudden drop to a rather low level, signaling a re-entrant transition near 80 °C from ordered to disordered micelles, followed by an increase in the viscosity presumably associated with the formation of micellar aggregates. This transition is driven by the diminishing solubility of the PEO corona chains in aqueous solution at sufficiently high temperature, and hence this sharp decrease differs from the long-range, pretransitional behavior observed at the low-temperature boundary of gel formation. We speculate that initially the diminished solubility of PEO chains leads to a gradual collapse of the micelle coronae and a concomitant reduction in the effective micelle volume fraction. This leads to enhanced fluidity of the solution and increased diffusivity of the latex probe particles, as seen in Figure 6. However, further decrease in solubility of PEO with rising temperature eventually leads to restructuring of the micellar solution into a more viscous phase and an abrupt decrease of probe particle mobility. Thus, the narrow region depicted with the two dashed lines in Figure 4 contains a low-viscosity liquid phase occurring immediately after the high-temperature gel phase boundary. The nature of the phase following this narrow, liquid-phase region is not clear. For certain Pluronic species, this phase corresponds to a morphologically new mesophase. For instance, in Pluronic P85 aqueous systems the cubic crystalline gel structure formed from spherical micelles eventually transforms with heating into a hexagonal mesophase formed from rod-like micelles.[52,53] Wu et al.[23] report that a lamellar phase is located beyond the cubic phase at higher temperatures and concentrations for F68 Pluronic, which has shorter chains than F108 but with the same 80% PEO composition as F108. Another likely possibility for the re-entrant viscosity increase in the micellar solution at temperatures higher than the gel-melting temperature is that weak attractive interactions between PEO chains lead to aggregates of spherical micelles. On approach to the cloud-point temperature, near 110 °C, a gradual decrease of the viscosity is observed and at the cloud-point temperature the viscosity decreases to rather low values. Nonmonotonic behavior of the viscosity for temperatures above the gel phase boundary could be a result of a series of complex morphology changes associated with micellar aggregation that occur with increasing temperature finally leading to macroscopic phase separation of the polymer at the cloud-point boundary.

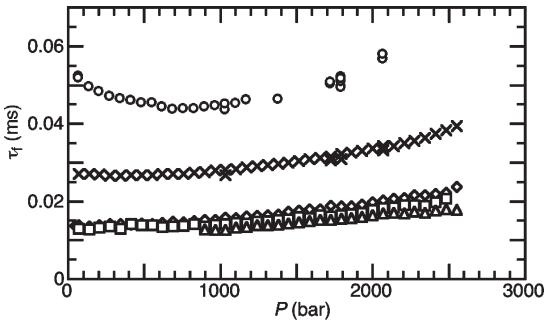

Figure 7. Pressure dependences of the decay time of the fast micellar mode, τ_f, for the 0.20 g/cm^3 F108 aqueous solution: diamonds, 22 °C; squares, 30 °C; triangles, 45 °C; crosses, 92 °C; circles, 102 °C. Scattering angle: 90°.

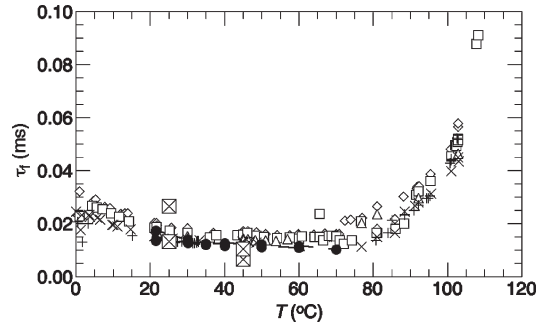

Figure 8. Temperature dependence of the decay time, τ_f, for the fast mode for the 0.20 g/cm^3 F108 aqueous solution with latex particles: crosses, 70 bar; times signs, 1035 bar; triangles, 1380 bar; squares, 1790 bar; diamonds, 2070 bar. The filled circles represent data for the 0.20 g/cm^3 F108 aqueous solution without latex particles. The crossed squares represent neutron spin echo data[16] for the fast mode after q^2 rescaling to the DLS scale. Scattering angle: 90°.

Collective Dynamics of Pluronic Solutions. Fast Mode. Figures 7 and 8 show the effects of pressure and temperature on the decay time of the fast mode, τ_f, which is the main dynamic mode of the aqueous Pluronic system. The behavior of this fast mode is qualitatively different from the diffusive dynamics of the latex probe particles shown in Figures 5 and 6. Figure 7 shows that for temperatures from 22 to 92 °C, τ_f is a monotonically increasing function of pressure, while at 102 °C (near the cloud-point boundary), τ_f initially decreases with pressure until reaching a local minimum at approximately 750 bar. Note also that τ_f is relatively insensitive to temperature between 22 and 45 °C, but is a much stronger function of temperature at 92 and 102 °C. Because the pressure dependence of τ_f appears to be rather weak, it is informative to depict the temperature dependence of τ_f in Figure 8 for all of the pressures explored. Both Figures 7 and 8 show that τ_f is insensitive to the increase of viscosity revealed by the latex probe particles (Figures 5 and 6). The magnitude of τ_f is rather insensitive to the proximity of either the gel transition or the critical micellization line. This behavior is in agreement with the observations of Pan et al.[54] The low-pressure values of τ_f, obtained at 45 °C in the vicinity of the gel-phase boundary, are almost the same as the values obtained at 22 °C far from this boundary (Figure 7). Moreover, the magnitude of τ_f is also insensitive to the nonmonotonic pressure dependence of the scattering intensity (another measure of the phase behavior of the micellar solution) shown in Figure 3.

At low temperatures, below the critical micellization temperature, the solution is composed of individual polymer

chains, implying that the fast mode at these temperatures represents the cooperative dynamics of concentration fluctuations of polymer chains in solution. The initial gradual decrease of τ_f with the increase of temperature (Figure 8) most plausibly is driven by a common Arrhenius dependence similar to that noticed for the latex probe particle dynamics at low temperatures. With further increase of temperature, the polymer chains begin to assemble into micelles in equilibrium with a progressively decreasing fraction of individual polymer chains. The rather smooth behavior of the data exhibited in Figures 7 and 8 suggests that the fast mode originates from polymer concentration fluctuations in the entire pressure and temperature range regardless of the state of aggregation of the PPO blocks and of the phase of the Pluronic micelles. Thus, the main contributor to these fluctuations should be the water-soluble PEO blocks given the large ratio of EO to PO monomer units. PEO blocks occupy a major fraction of the micellar system volume, while the PPO blocks have the tendency to collapse into globules. In particular, the similarity of the behavior of the fast mode in the gel phase and in the concentrated liquid micellar phase that precedes it indicates that these concentration fluctuations depend primarily on the local solution microenvironment in the PEO coronae of the micelles and not on the arrangement of the micelles. This view is supported by the results of neutron spin echo (NSE) studies of Yardimci et al.,[16] which show that the intermediate scattering functions characterizing chain dynamics of F68 and F108 Pluronic solutions was insensitive to the phase (liquid or gel) of the Pluronic system.

Further evidence of the localized nature of the fast dynamics can be found by comparing DLS data for samples with and without added probe particles. Figure 8 also shows τ_f data for solutions without probe particles in the temperature range where the micellar system forms the nonergodic gel phase. These measurements are performed without ensemble averaging, which normally is necessary for such a nonergodic system. However, these time-averaged data for the probe-free samples are still meaningful since the contribution of "frozen" scatterers in the sample without latex particles appears to be relatively low (Figure 1). Figure 8 shows that the fast mode relaxation times for a solution at ambient pressure, which forms a gel between about 30 and 80 °C, are close to the values obtained in the liquid state at high pressure. Moreover, the data in Figure 8 indicate no detectable change in the behavior of the fast mode in solution without probe particles throughout the gel regime between about 30 and 80 °C. Therefore, the fast mode is expected to represent motion at length scales smaller than the characteristic spacing between micelles of the gel network (~20 nm for F108). Assuming that the fast mode is related to concentration fluctuations, a characteristic fluctuation length, ξ, can be extracted from the fast mode data using the standard expression for semidilute polymer solutions: $\tau_f = (D_c q^2)^{-1}$ with the diffusion coefficient D_c given by

$$D_c = \frac{k_B T}{6\pi\eta\xi} \tag{2}$$

where viscosity η is related to the length scale of concentration fluctuations and may differ from viscosity η_{app} revealed by the latex probe particles. In order to get an upper bound on ξ for a given τ_f, the viscosity of pure water is used as the lowest estimate for η. An upper limit for the fast mode correlation length, $\xi < 3$ nm, is found using $\tau_f = 20$ μs as an upper limit on the fast mode relaxation time in the gel regime (~30−80 °C in Figure 8). The upper limit for ξ is much less

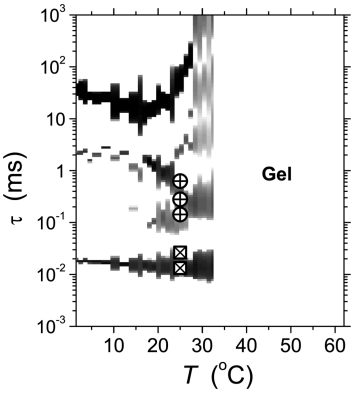

Figure 9. Temperature dependence of the decay time distribution represented in log-grayscale for the 0.20 g/cm^3 F108 aqueous micellar system at ambient pressure and at temperatures below the gelation boundary. Also shown are neutron spin echo (NSE) data for the 0.21 g/cm^3 F108 aqueous system at ambient pressure and 25 °C. The crossed squares represent the NSE fast dynamic mode and the crossed circles represent the NSE slow dynamic mode,[16] both after q^2 rescaling to the DLS scale. DLS scattering angle: 90°.

than the micelle diameter, which is the characteristic length scale of the concentrated liquid and gel micelle phases. In a cubic crystalline gel, each lattice point is represented by a spherical micelle trapped by neighbors in an entangled polymer network of micellar coronas. Here we argue that the fast mode represents the cooperative dynamics of polymer chains regardless of whether or not the chains are included in micellar coronas or exist as free chains and regardless if the system is in the liquid or gel states. This conclusion is in agreement with the results from fluorescent probe studies of F88 aqueous systems by Grant et al.[33,34]

Note that the thermal motion of the coronae PEO chains, corresponding to the fast mode provides a source of entropy production that counteracts the loss of translational entropy associated with the formation of an ordered micellar gel phase at elevated temperature. This mechanism, together with the increase of entropy associated with the loss of water structure around the Pluronic chains, insures that in spite of the transition to an ordered crystalline state the total system entropy increases with heating as suggested by Mortensen et al.[13] and as required by thermodynamics.

Comparison of DLS and NSE Data for Fast and Slow Dynamics. It is interesting to compare the dynamics of 0.21 g/cm^3 F108 micellar system in D_2O probed by NSE reported by Yardimci et al.[16] with the dynamics of the 0.20 g/cm^3 F108 in water probed by DLS reported in this paper. The probe scale for the NSE measurements, $2\pi/q$, ranges from 5.3 to 6.9 nm, while for DLS measurements at the scattering angle of 90° the probe scale is $2\pi n/q = 376$ nm. Two dynamic modes are observed in the NSE study.[16] The fast NSE mode is a diffusion mode with the decay-time proportional to q^{-2}. This fast NSE mode can be compared with the fast DLS mode after q^2 rescaling: $\tau_{eff} = \tau_{NSE}(q_{NSE}/q_{DLS})^2$. Figure 8 shows that the DLS data for τ_f are in good agreement with the fast dynamic mode obtained at 25 and 45 °C with NSE[16] and data rescaled with q^2.

Figures 9−11 show the behavior of the DLS modes in comparison with the fast and the slow NSE modes. It has been reported[16] that the slow NSE mode exhibits a stronger than quadratic dependence on the wavenumber q and is attributed to the slow motion in the micellar core. The slow satellite modes, revealed in the DLS measurements, exhibit rather complex temperature and pressure behavior, which appears to be correlated with the micellization and gelation

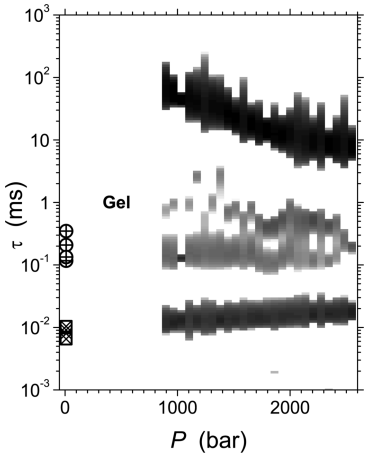

Figure 10. Pressure dependence of the decay time distribution represented in log-grayscale for the 0.20 g/cm^3 F108 aqueous micellar system at 45 °C. Also shown are neutron spin echo (NSE) data for the 0.21 g/cm^3 F108 aqueous system at 45 °C. The crossed squares represent the NSE fast dynamic mode and the crossed circles represent the NSE slow dynamic mode,[16] both after q^2 rescaling to the DLS scale. DLS scattering angle: 90°.

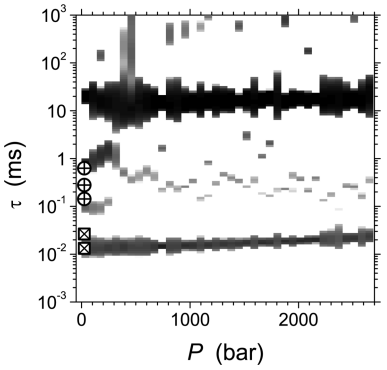

Figure 11. Pressure dependence of the decay time distribution represented in log-grayscale for the 0.20 g/cm^3 F108 aqueous micellar system at 22 °C. Also shown are neutron spin echo (NSE) data for the 0.21 g/cm^3 F108 aqueous system at 25 °C. The crossed squares represent the NSE fast dynamic mode and the crossed circles represent the NSE slow dynamic mode,[16] both after q^2 rescaling to the DLS scale. DLS scattering angle: 90°.

phase transitions. At low temperatures where the solution contains individual polymer chains, the single slow mode could be attributed as a "heterogeneity mode", following the notation of Pan et al.[54] Additional dynamic modes are observed in the micellar phase. The NSE decay time data, corresponding to three q values, are rescaled with q^2 and plotted on top of our DLS data. The DLS data are plotted in the two-dimensional graphs as the decay time distributions $H(\tau)$ at various temperatures and pressures with the magnitude of a distribution shown in a grayscale for convenience of representation as adopted in our previous papers.[55,56] The grayscale is logarithmic here to enhance the visualization of the weak slow modes. All distributions are normalized to the equal integral over the logarithmic decay-time scale. The view of the entire picture of the sequence of distributions obtained at gradually varied temperature or pressure tends to average the uncertainties of each distribution and helps to reveal the trend of the dynamics, which is particularly essential for weak modes. The slowest mode results from the diffusion of latex probe particles. The fast intensive mode corresponds to concentration fluctuations. A variety of weak

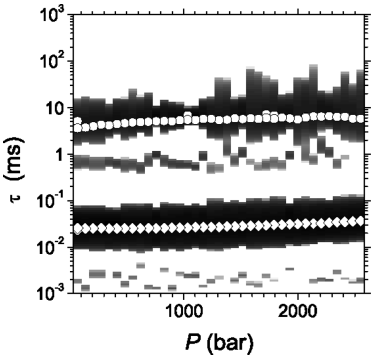

Figure 12. Pressure dependence of the decay time distribution represented in log-grayscale for the 0.20 g/cm^3 F108 aqueous micellar system at 92 °C. Fit to the sum of two exponentials: fast mode, diamonds; latex mode, circles. Scattering angle: 90°.

slow satellite modes are present between these two intensive modes. The rescaled data for the NSE slow mode[16] shown in Figures 9−11 are rather close to the DLS slow modes depicted in grayscale. This result supports the assumption of the similar nature of the NSE and, at least, some of the DLS slow modes. It should be noticed that the available accuracy of the NSE data is not high enough to distinguish more than a single slow mode. In contrast, DLS is able to resolve two or three slow modes as shown in the figures. Also, in spite of the rather strong q-dependence of the NSE slow mode reported by Yardimci et al.,[16] a conventional q^2 rescaling factor is justified because of the good match of the slow DLS modes with the NSE slow mode obtained with this scaling. Indeed, micellar core dynamics could exhibit coupling with dynamics of concentration fluctuations very similar to the coupling of dynamic modes in semidilute polymer solutions[55] where chain entanglements have effect. In a micellar system such coupling is possible as a result of the constrained motion in the micellar corona of the PEO blocks, which at one end are trapped in the entangled micellar PPO core. Thus, core dynamics at rather short length scales could be revealed not only in NSE but also in DLS measurements. The good match of the slow DLS modes with the q^2 rescaled NSE slow mode indicates that the strong q-dependence of the NSE slow mode is observed in a rather narrow range of wave numbers when the probe length is comparable with the size of the micellar core. It is not apparent that this strong q-dependence should remain in effect as the size of the probe length increases to that found with DLS. In fact, the conventional q^2 dependence is observed with DLS. The observed deviations of the NSE data from q^2 dependence are imperceptible in the logarithmic time scale, which spans several decades.

Figure 12 shows the evolution of dynamic modes with pressure at 92 °C, which is above the gel-melting boundary. The main fast mode, which is attributed to concentration fluctuations, looks rather wide in the logarithmic grayscale graph. This results from the high intensity of this mode in the close proximity to the cloud-point boundary, which is found at 110 °C. Figure 12 also shows the fit of the correlation functions to the sum of two exponentials neglecting the weak mode contributions, overlaid on the distributions to demonstrate how the two main modes are resolved. The satellite modes between the main modes are rather weak and it is difficult to resolve them in fitting to additional exponentials. An additional weak, fast dynamic mode emerges at the microsecond scale, which is faster than the main fast mode. This fastest mode is so weak and unstable that it is natural to consider it a ghost of the ill-posed inverse Laplace transform.

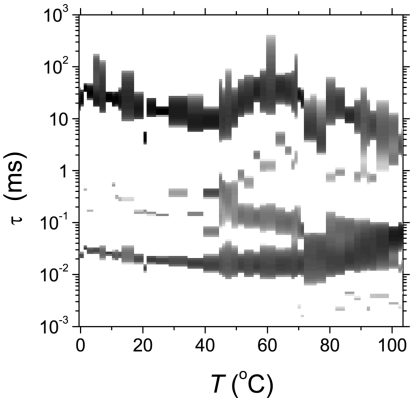

Figure 13. Temperature dependence of the decay time distribution represented in log-grayscale for the 0.20 g/cm^3 F108 aqueous micellar system at 2070 bar. Scattering angle: 90°.

However, this mode is not detected in all other phases below 80 °C, which is a strong argument that the mode is real. Indeed a similar dynamic mode has been found by Schillen et al.[52] in dilute P85 solutions and has been attributed to the rotational diffusion of rod-like micelles. However, it remains unclear why the neutron scattering data,[16] for the F108 Pluronic system used in the present study, did not provide direct evidence of a change of symmetry of the mesophase upon heating. The same weak, fast mode is found at temperatures greater than 80 °C in Figure 13, which demonstrates changes in dynamics with temperature at a pressure of 2070 bar, well above the critical pressure of gelation.

Figure 13 shows that in the liquid-phase region with spherical micelles and micellar clusters, satellite mode splitting into two separate dynamic modes is observed. It is interesting that the slower of these two modes mimics the dynamics of the latex probe particles, while the other mode does not obey the apparent viscosity changes and becomes faster with viscosity increase. We speculate that the slower satellite mode could be related to the deformation relaxation of the gel clusters responding to collisions.

Pretransitional Fluctuations. Figure 8 shows that the fast mode exhibits pretransitional slowing down on approach to the cloud point temperature, T^*. This behavior is a characteristic of second order phase transitions. The correlation length ξ of the concentration fluctuations in the vicinity of critical point obeys a power law scaling with the Ising critical exponent $\nu = 0.63$. In accordance with eq 2 the decay time for the fast mode, τ_f, is proportional to $\xi\eta/T$. The microscopic viscosity η is related to the length scale of the concentration fluctuations and is different from the viscosity η_{app} revealed by the latex probe. Since the viscosity η is not available, the behavior of τ_f is compared directly with predicted power law behavior assuming that, in the first approximation, the temperature dependence of η/T between 50 and 110 °C can be neglected. This approximation is rather rough given, for instance, that η/T for water decreases by a factor of 2 in this temperature interval.

Figure 14 shows a log−log plot of the τ_f data at 1790 bar and temperatures above 50 °C as a function of the reduced temperature distance to the cloud point, $\varepsilon = (T^* - T)/T$, where T is the absolute temperature. This figure shows that the behavior of τ_f in the broad vicinity of the cloud point is similar to that exhibited by the critical dynamics of concentration fluctuations.

Such critical scaling far from the cloud point is also evident in the behavior of the scattering intensity, I_m, of the micellar system (Figure 3). Figure 15 shows the intensity of scattering

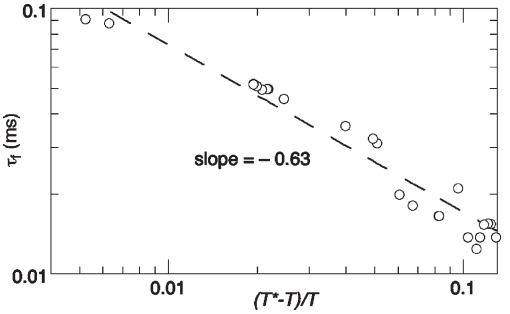

Figure 14. Log−log plot for the fast mode decay time, τ_f, for the 0.20 g/cm^3 F108 aqueous system at 1790 bar on approach to the cloud-point temperature, $T^* = 110$ °C. The dashed line, with a slope of −0.63, is shown for comparison.

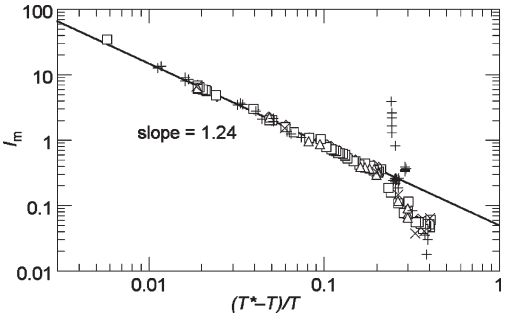

Figure 15. Scattering intensity, I_m, as a function of the reduced temperature on approach to the cloud point, T^*, and various pressures for the 0.20 g/cm^3 F108 aqueous system: crosses, 70 bar; times signs, 1035 bar; triangles, 1380 bar; squares, 1790 bar; diamonds, 2070 bar. $T^* = 107$ °C at 70 bar and $T^* = 110$ °C at higher pressures. Scattering angle: 90°.

by the Pluronic solution at different pressures as a function of the reduced temperature distance, ε. The cloud-point temperature, $T^* = 110$ °C, corresponding to the observed value at 1790 bar, is adopted for all but the lowest pressure of 70 bar, where $T^* = 107$ °C is used. The reduction of T^* at the lowest pressure is consistent with the increase of the scattering intensity at 102 °C at ambient pressure shown in Figure 3.

The cloud-point temperature appears to be almost independent of pressure (see Figure 4), which is in agreement with literature data for the phase separation boundary of PEO in water.[57,58] However, the data of Cook et al.[57] and Sun and King[58] show that the $P-T$ trace of the PEO−water cloud-point curve has a slight negative slope at temperatures from ∼100 to ∼0 °C where the curve then exhibits a maximum, $(\partial P/\partial T)_{concentration} = 0$, at a pressure of ∼4500−5600 bar, depending on polymer concentration and molecular weight. As the temperature is lowered further the $P-T$ trace of the PEO−water cloud-point curve exhibits a fairly large positive slope. Hence, the single-phase region for the PEO−water solution exists at temperatures below ∼100 °C and pressures below ∼5600 bar. Since Pluronic F108 has 80 mass % PEO, it is reasonable to expect the $P-T$ trace of the cloud-point curve for this Pluronic-water system also to exhibit a maximum at a pressure in excess of the high pressure limit of the apparatus used in the present study.

Figure 15 shows that the static light scattering in this Pluronic system is also described well by power-law behavior, with the Ising critical exponent $\gamma = 1.24$. Somewhat surprisingly, this conventional pretransitional critical behavior is valid over a very broad range of temperatures starting from about 40 °C to the cloud point at 110 °C. However, there is a fundamental reason for such behavior. The cloud

point for this Pluronic aqueous system should be close to the phase separation transition for an aqueous solution with a low molecular weight PEO. It is well-known that the asymmetry of the phase boundary for a low molecular weight polymer is low. Therefore, it is quite possible that the polymer volume fraction for our sample, ~ 0.2, is rather close to the critical concentration corresponding to the maximum of the boundary. It is also well-known that even significant deviations of the polymer concentration from the critical value usually do not have much affect on the criticality of the sample. The near-critical polymer concentration of our sample can explain the very broad temperature range of critical behavior of the sample.

It should be noted that a micellar system has an additional length parameter, which is the size of the micelles. The critical behavior of such systems should exhibit a crossover from the mean-field regime ($\gamma = 1.0$), far from the critical point, to the Ising-like regime ($\gamma = 1.24$), close to the critical point, similar to the critical behavior in polymer solutions.[59] However, this crossover behavior is not observed in the intensity data in Figure 15. It is plausible that the detection of crossover critical phenomena is beyond the rather limited accuracy available for the scattering intensity data obtained from DLS measurements.

Below 40 °C the scattering intensity drastically deviates from this power law behavior. It is interesting that gel formation and melting have no apparent affect on the power law behavior of the scattering intensity of this micellar system, while the apparent viscosity changes dramatically with gelation. Note that this observation is related to the intensity of scattering at the angle of 90°, while the speckle at low angles becomes bright at gel formation and melting, reflecting large-scale changes in the mesophase behavior. Our observation of power law behavior of the scattering intensity is consistent with the results reported in ref 31 for Pluronic L64 solutions, where power law behavior has been detected in a significantly narrower temperature interval using a conventional static light scattering method. The cooperative dynamics of polymer chains at the length scales of the concentration fluctuations observed in a very broad temperature interval is partially responsible for the production of entropy ensuring that the total system entropy increases even though an ordered gel phase appears.

It is interesting that the same power law behavior of the scattering intensity covers quite different areas of the phase diagram (areas 3 and 5 in Figure 4), which are separated with a narrow gap close to 80 °C where the effective viscosity sharply decreases. Regions 3 and 5 of the phase diagram contain liquid but the micelles in these regions are expected to be organized differently (i.e., ordered cubic arrangements in the main gel phase vs micellar aggregates and possibly network structures at higher temperature). While the exponent of the critical power law, $\gamma = 1.24$, is universal, the amplitude is system dependent and should be different for phases with different structural arrangements of the micelles. However, it is plausible that while the micellar order is different for these phases, the local concentration fluctuations of the PEO micelle coronae are insensitive to the micellar superstructure, as suggested by the NSE studies.[16]

Summary

The pressure−temperature phase behavior for the 0.20 g/cm^3 Pluronic F108 aqueous system exhibits several phase transformations at high concentrations including a transition from a liquid to a gel phase and a subsequent re-entrant transition from the gel phase to a liquid phase with increasing temperature. The temperature range spanning the gel phase is a decreasing function of pressure, which vanishes at a critical value of pressure. The pressure trace of the high-temperature gel-melting phase boundary steeply decreases with an increase of temperature, and is almost parallel to the cloud-point curve, which itself exhibits rather weak pressure dependence. The similarity of the pressure behavior of the cloud-point and the high-temperature gel-melting phase boundary transitions can be explained by forcing PEO blocks out of water. In contrast, the pressure at the low-temperature gelation boundary gradually increases with temperature similar to the critical micellization line and to the line of termination of micellization. The pressure behavior of these phase boundaries is determined mainly by the increase of solubility of PPO blocks in water under pressure.

Latex probe nanoparticles doped in the aqueous Pluronic system provide a means to locate the phase transition boundaries and to map the phase diagram. Along with the apparent local viscosity and the intrinsic collective dynamics of the Pluronic solutions, information is obtained on the intensity of scattering by the Pluronic system using DLS measurements only. The local solution viscosity exhibits nonmonotonic behavior as a function of temperature and pressure due to changes in the phase or microstructure of the system. At temperatures above the gel-melting boundary a region exists with elevated viscosity attributed to the aggregation of micelles in the vicinity of a second gel phase that could possibly form at higher F108 concentrations. In the entire range of pressures explored in this study, the micellar scattering intensity exhibits critical pretransitional temperature dependence over a broad temperature interval that spans the gel phase. The surprisingly fair quality of the revealed critical behavior of the scattering intensity confirms the validity of the method of intensity evaluation based on DLS data.

The intrinsic dynamics of the Pluronic solutions exhibit several modes, including a dominant diffusive mode of concentration fluctuations with critical behavior in a broad temperature interval including the gel phase. The characteristic length scale of these fluctuations below the gel-melting transition is an order of magnitude lower than the spacing between micelles in the ordered crystalline structure of the gel phase. The entropy increase related to these fluctuations is assumed to be a counter to the entropy decrease with ordering of the micellar system at gelation.

Satellite dynamic modes are rather weak as compared with the main mode of concentration fluctuations. The satellite dynamic modes apparently exhibit q^2 dependence. Below the gel-melting boundary the satellite modes appear as slow modes, which exhibit complex behavior with temperature and pressure depending on the physical state of the system. In the two-phase region, where finite gel clusters emerge in a micellar liquid, one of the slow modes mimics the viscosity changes. This mode could be attributed to deformation relaxation of the gel clusters caused by their collisions.

Acknowledgment. The authors are grateful to BASF for providing Pluronic F108 for our experiments as a gift. J.L.H. acknowledges support from an NSERC Discovery grant.

Supporting Information Available: Text and figures showing additional pressure and temperature dependences of the decay time distributions on the investigated Pluronic system and a figure showing correlation functions at various temperatures. This material is available free of charge via the Internet at http://pubs.acs.org.

References and Notes

(1) Matsuyama, A.; Tanaka, F. *Phys. Rev. Lett.* **1990**, *65*, 341–344.
(2) Bekiranov, S.; Bruinsma, R.; Pincus, P. *Phys. Rev. E* **1997**, *55*, 577–585.

(3) Mortensen, K. *Polym. Adv. Technol.* **2001**, *12*, 2–22.
(4) Mortensen, K. *Colloids Surf., A* **2001**, *183*, 277–292.
(5) Kabanov, A. V.; Batrakova, E. V.; Alakhov, V. Y. *J. Controlled Release* **2002**, *82*, 189–212.
(6) Mortensen, K.; Brown, W.; Norden, B. *Phys. Rev. Lett.* **1992**, *68*, 2340–2343.
(7) Wanka, G.; Hoffmann, H.; Ulbricht, W. *Macromolecules* **1994**, *27*, 4145–4159.
(8) Mortensen, K.; Talmon, Y. *Macromolecules* **1995**, *28*, 8829–8834.
(9) Mortensen, K. *J. Phys.: Condens. Matter* **1996**, *8*, A103–A124.
(10) Bahadur, P. *Curr. Sci.* **2001**, *80*, 1002–1007.
(11) Wu, Y. L.; Sprik, R.; Poon, W. C. K.; Eiser, E. *J. Phys.: Condens. Matter* **2006**, *18*, 4461–4470.
(12) Pandit, N. K.; Kisaka, J. *Int. J. Pharm.* **1996**, *145*, 129–136.
(13) Mortensen, K.; Schwahn, D.; Janssen, S. *Phys. Rev. Lett.* **1993**, *71*, 1728–1731.
(14) Hvidt, S. *Colloids Surf., A* **1996**, *112*, 201–207.
(15) Thiyagarajan, P. *J. Appl. Crystallogr.* **2003**, *36*, 373–380.
(16) Yardimci, H.; Chung, B.; Harden, J. L.; Leheny, R. L. *J. Chem. Phys.* **2005**, *123*, 244908.
(17) Brown, W.; Schillen, K.; Almgren, M.; Hvidt, S.; Bahadur, P. *J. Phys. Chem.* **1991**, *95*, 1850–1858.
(18) Brown, W.; Schillen, K.; Hvidt, S. *J. Phys. Chem.* **1992**, *96*, 6038–6044.
(19) Bahadur, P.; Pandya, K. *Langmuir* **1992**, *8*, 2666–2670.
(20) Almgren, M.; Bahadur, P.; Jansson, M.; Li, P. Y.; Brown, W.; Bahadur, A. *J. Colloid Interface Sci.* **1992**, *151*, 157–165.
(21) Almgren, M.; Brown, W.; Hvidt, S. *Colloid Polym. Sci.* **1995**, *273*, 2–15.
(22) Schillen, K.; Brown, W.; Konak, C. *Macromolecules* **1993**, *26*, 3611–3614.
(23) Wu, G. W.; Chu, B. *Macromolecules* **1994**, *27*, 1766–1773.
(24) Zhou, Z.; Chu, B. *Macromolecules* **1994**, *27*, 2025–2033.
(25) Nystrom, B.; Walderhaug, H.; Hansen, F. K. *Faraday Discuss.* **1995**, *101*, 335–344.
(26) Nystrom, B.; Kjoniksen, A. L. *Langmuir* **1997**, *13*, 4520–4526.
(27) Yuan, G. C.; Wang, X. H.; Han, C. C.; Wu, C. *Macromolecules* **2006**, *39*, 3642–3647.
(28) Wolff, M.; Magerl, A.; Frick, B.; Zabel, H. *Phys. Rev. E* **2005**, *71*, 011509.
(29) Prudhomme, R. K.; Wu, G. W.; Schneider, D. K. *Langmuir* **1996**, *12*, 4651–4659.
(30) Hvidt, S.; Jorgensen, E. B.; Brown, W.; Schillen, K. *J. Phys. Chem.* **1994**, *98*, 12320–12328.
(31) Lobry, L.; Micali, N.; Mallamace, F.; Liao, C.; Chen, S. H. *Phys. Rev. E* **1999**, *60*, 7076–7087.
(32) Jeon, S.; Granick, S.; Kwon, K. W.; Char, K. *J. Polym. Sci., Part B: Polym. Phys.* **2002**, *40*, 2883–2888.
(33) Grant, C. D.; DeRitter, M. R.; Steege, K. E.; Fadeeva, T. A.; Castner, E. W. *Langmuir* **2005**, *21*, 1745–1752.
(34) Grant, C. D.; Steege, K. E.; Bunagan, M. R.; Castner, E. W. *J. Phys. Chem. B* **2005**, *109*, 22273–22284.
(35) Kermis, T. W.; Li, D.; Guney-Altay, O.; Park, I. H.; van Zanten, J. H.; McHugh, M. A. *Macromolecules* **2004**, *37*, 9123–9131.
(36) Li, D.; McHugh, M. A.; van Zanten, J. H. *Macromolecules* **2005**, *38*, 2837–2843.
(37) Lemmon, E. W.; McLinden, M. O.; Friend, D. G., *Thermophysical Properties of Fluid Systems in NIST Chemistry WebBook*; National Institute of Standards and Technology: Gaithersburg MD, 2005.
(38) Schiebener, P.; Straub, J.; Sengers, J.; Gallagher, J. S. *J. Phys. Chem. Ref. Data* **1990**, *19*, 677–717.
(39) Alargova, R. G.; Deguchi, S.; Tsujii, K. *Colloids Surf., A* **2001**, *183−185*, 303–312.
(40) Meier, G.; Vavrin, R.; Kohlbrecher, J.; Buitenhuis, J.; Lettinga, M. P.; Ratajczyk, M. *Meas. Sci. Technol.* **2008**, *19*, 034017.
(41) Alexandridis, P.; Nivaggioli, T.; Hatton, T. A. *Langmuir* **1995**, *11*, 1468–1476.
(42) Pusey, P. N.; Vanmegen, W. *Physica A* **1989**, *157*, 705–741.
(43) Castelletto, V.; Hamley, I. W.; Waigh, T. A. *J. Chem. Phys.* **2004**, *121*, 11474–11480.
(44) Bohidar, H. B. *Curr. Sci.* **2001**, *80*, 1008–1017.
(45) Bohorquez, M.; Koch, C.; Trygstad, T.; Pandit, N. *J. Colloid Interface Sci.* **1999**, *216*, 34–40.
(46) Zhou, Z. K.; Chu, B. *Macromolecules* **1987**, *20*, 3089–3091.
(47) Zhou, Z. K.; Chu, B. *Macromolecules* **1988**, *21*, 2548–2554.
(48) Mortensen, K.; Batsberg, W.; Hvidt, S. *Macromolecules* **2008**, *41*, 1720–1727.
(49) Alexandridis, P.; Holzwarth, J. F.; Hatton, T. A. *Macromolecules* **1994**, *27*, 2414–2425.
(50) Lau, B. K.; Wang, Q. Q.; Sun, W.; Li, L. *J. Polym. Sci., Part B: Polym. Phys.* **2004**, *42*, 2014–2025.
(51) Li, Y. Q.; Shi, T. F.; Sun, Z. Y.; An, L. J.; Huang, Q. R. *J. Phys. Chem., B* **2006**, *110*, 26424–26429.
(52) Schillen, K.; Brown, W.; Johnsen, R. M. *Macromolecules* **1994**, *27*, 4825–4832.
(53) Jorgensen, E. B.; Hvidt, S.; Brown, W.; Schillen, K. *Macromolecules* **1997**, *30*, 2355–2364.
(54) Pan, C.; Maurer, W.; Liu, Z.; Lodge, T. P.; Stepanek, P.; Vonmeerwall, E. D.; Watanabe, H. *Macromolecules* **1995**, *28*, 1643–1653.
(55) Kostko, A. F.; Anisimov, M. A.; Sengers, J. V. *Phys. Rev. E* **2002**, *66*, 020803.
(56) Kostko, A. F.; Anisimov, M. A.; Sengers, J. V. *Phys. Rev. E* **2007**, *76*, 021804.
(57) Cook, R. L.; King, H. E.; Peiffer, D. G. *Phys. Rev. Lett.* **1992**, *69*, 3072–3075.
(58) Sun, T.; King, H. E. *Macromolecules* **1998**, *31*, 6383–6386.
(59) Anisimov, M. A.; Kostko, A. F.; Sengers, J. V.; Yudin, I. K. *J. Chem. Phys.* **2005**, *123*, 164901.